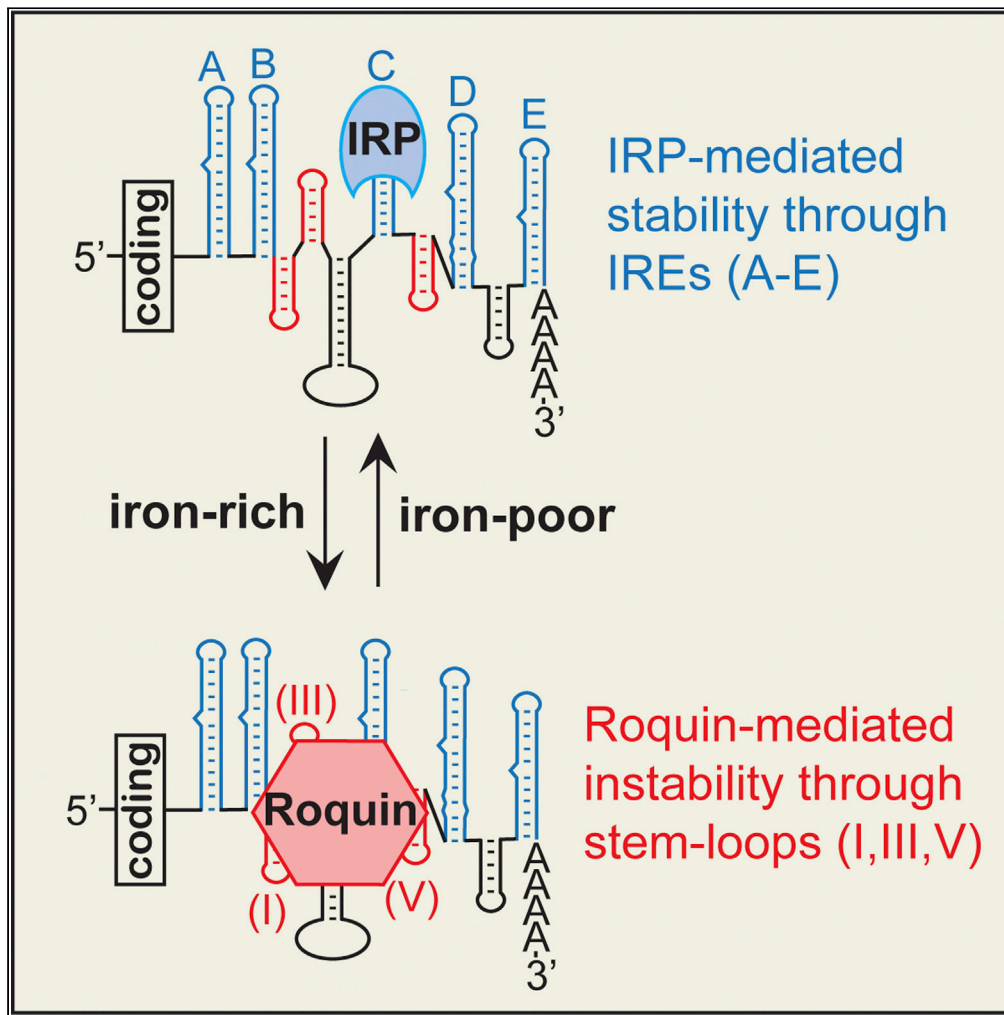


Article

Roquin is a major mediator of iron-regulated changes to transferrin receptor-1 mRNA stability



Victor M. Corral,  
Eric R. Schultz,  
Richard S.  
Eisenstein,  
Gregory J. Connell

conne018@umn.edu

Highlights

Roquin is a major mediator of iron-regulated TfR1 mRNA instability

Roquin-mediated instability requires three stem loops within the TfR1 3'-UTR

Iron-regulated TfR1 mRNA instability can occur in the absence of Regnase-1



## Article

## Roquin is a major mediator of iron-regulated changes to transferrin receptor-1 mRNA stability

Victor M. Corral,<sup>1,3</sup> Eric R. Schultz,<sup>1,3</sup> Richard S. Eisenstein,<sup>2</sup> and Gregory J. Connell<sup>1,4,\*</sup>

## SUMMARY

**Transferrin receptor-1 (TfR1) has essential iron transport and proposed signal transduction functions. Proper TfR1 regulation is a requirement for hematopoiesis, neurological development, and the homeostasis of tissues including the intestine and muscle, while dysregulation is associated with cancers and immunodeficiency. TfR1 mRNA degradation is highly regulated, but the identity of the degradation activity remains uncertain. Here, we show with gene knockouts and siRNA knockdowns that two Roquin paralogs are major mediators of iron-regulated changes to the steady-state TfR1 mRNA level within four different cell types (HAP1, HUVEC, L-M, and MEF). Roquin is demonstrated to destabilize the TfR1 mRNA, and its activity is fully dependent on three hairpin loops within the TfR1 mRNA 3'-UTR that are essential for iron-regulated instability. We further show in L-M cells that TfR1 mRNA degradation does not require ongoing translation, consistent with Roquin-mediated instability. We conclude that Roquin is a major effector of TfR1 mRNA abundance.**

## INTRODUCTION

The transferrin receptor (TfR1, TFRC) is the major mechanism for iron importation in proliferating mammalian cells. It also has roles that are independent of Fe(III)-transferrin interactions and possibly involve several different signal transduction pathways (Chen et al., 2015; Coulon et al., 2011; Pham et al., 2014; Salmeron et al., 1995; Senyilmaz et al., 2015). The importance of TfR1 is supported by the non-viability of *Tfrc*<sup>-/-</sup> null mice (Levy et al., 1999) as well as by rare anemias that can result in patients that either express autoantibodies to the receptor (Larrick and Hyman, 1984), have reduced TfR1 expression (Hao et al., 2015), or have a TfR1 missense mutation that disrupts receptor internalization (Jabara et al., 2016). The missense mutation also results in chronic immunodeficiency, further emphasizing the importance of the receptor, particularly in proliferating cells. TfR1 is also essential for cardiac and skeletal muscle (Barrientos et al., 2015; Xu et al., 2015), dopaminergic neurons (Matak et al., 2016), intestinal epithelium (Chen et al., 2015), and most likely insulin synthesis (Santos et al., 2020). In contrast, elevated TfR1 expression contributes to iron overload in  $\beta$ -thalassemia (Li et al., 2017) and has long been associated with cancers (reviewed in Shen et al., 2018).

Although TfR1 regulation can occur transcriptionally (Casey et al., 1988a; Lok and Ponka, 1999; Tacchini et al., 1999), control of mRNA stability is the major mechanism through which TfR1 mRNA levels are altered in response to cellular iron requirements (Bayeva et al., 2012; Casey et al., 1988a; Owen and Kuhn, 1987). TfR1 mRNA stability is modulated through the interaction of iron regulatory proteins (IRPs) with iron-responsive elements (IREs), which are conserved bulged hairpin loop structures (reviewed in Galaris et al., 2019; Ghosh et al., 2015). TfR1 mRNA contains five IREs within its 3'-UTR that are labeled A-E (Casey et al., 1988b), and the binding of the IRPs (*ACO1* and *IREB2*) to these elements in some manner protects the mRNA from an endonuclease activity, leading to increased iron uptake. In the presence of iron, the RNA binding of the IRPs is attenuated through either modification or degradation. This results in increased TfR1 mRNA degradation and decreased iron uptake. A ~200 nt sequence within the 3'-UTR of TfR1 mRNA, which includes IREs B-D, was found to be sufficient to induce iron-regulated instability equivalent to that of the full-length mRNA (Casey et al., 1989; Mullner and Kuhn, 1988). Three non-IRE hairpin loops (I,III,V) were subsequently identified within this region that can account for most of the instability that occurs in the absence of IRP binding to the IREs. This suggested that the three non-IRE hairpin loops

<sup>1</sup>Department of Pharmacology, University of Minnesota, Minneapolis, MN 55455, USA

<sup>2</sup>Department of Nutritional Sciences, University of Wisconsin, Madison, WI 53706, USA

<sup>3</sup>These authors contributed equally

<sup>4</sup>Lead contact

\*Correspondence: [conne018@umn.edu](mailto:conne018@umn.edu)

<https://doi.org/10.1016/j.isci.2021.102360>



could be functioning as recognition elements for the iron-regulated degradation activity (Rupani and Connell, 2016).

Members of the Roquin and Regnase/MCPIP families of RNA binding proteins have the specificity for hairpin loops that is expected of a mediator of Tfr1 mRNA instability (Braun et al., 2018; Wawro et al., 2019; Yoshinaga et al., 2017). The Roquin family consists of two highly similar paralogs, Roquin-1 (*RC3H1*) and Roquin-2 (*RC3H2*), that were initially identified as inducing the instability of mRNAs encoding components of the adaptive immune system and have since been suggested to modulate a large number of other mRNAs (Braun et al., 2018; Vinuesa et al., 2005). Neither Roquin paralog is an endonuclease but rather induces mRNA decay by recruiting deadenylation and decapping complexes within processing bodies (Glasmacher et al., 2010; Mino et al., 2015). Roquin-induced mRNA decay is dependent upon an interaction with either trinucleotide loops (Leppke et al., 2013), referred to as constitutive decay elements, or with uridine-rich loop sequences (Janowski et al., 2016; Murakawa et al., 2015; Rehage et al., 2018). In contrast to the Roquin family, Regnase-1 (*ZC3H12A*) has intrinsic endonuclease activity and degrades translationally active mRNAs (reviewed in Yoshinaga and Takeuchi, 2019). It is the best characterized member of the Regnase/MCPIP family, which contains four members (Liang et al., 2008; Matsushita et al., 2009): Regnase1-4/MCPIP1-4 (*ZC3H12A-D*). Regnase-1 and Roquin regulate overlapping subsets of mRNAs, but they are structurally different and interact with the RNA stem loops through distinct mechanisms (Tan et al., 2014; Yokogawa et al., 2016), resulting in some unique specificities (Jeltsch et al., 2014; Mino et al., 2015). Although Regnase-1 was proposed to be a major mediator of iron-regulated Tfr1 mRNA degradation (Yoshinaga et al., 2017), we demonstrate here that the majority of the regulation is instead mediated by the two Roquin paralogs in each of the four cell types that were tested. The identification of the mechanism of iron-responsive Tfr1 mRNA instability is critical to understanding iron homeostasis and to the hematological, neurological, oncological, and other pathologies related to aberrant Tfr1 expression (reviewed in Nakamura et al., 2019).

## RESULTS

### Testing the relevance of *ZC3H12A-C* and *RC3H1-2* to the steady-state level of Tfr1 mRNA

A clustered regularly interspaced short palindromic repeats (CRISPR) knockout (KO) was made to each of the *ZC3H12A-C* and *RC3H1-2* family members to initially assess whether the proteins impact Tfr1 mRNA abundance (Figure 1). The KOs were made in the HAP1 cell line, which was derived from a patient with chronic myelogenous leukemia and is near haploid (Essletzbichler et al., 2014). Sequencing confirmed that each open reading frame was disrupted as intended by the CRISPR KO (transparent methods). The expression of Regnase-1 within the *ZC3H12A* KO is not detectable by Western analysis (Figure 1A), even after treatment of the cells with either deferoxamine (DFO), an iron chelator earlier shown to stimulate *ZC3H12A* transcription (Yoshinaga et al., 2017), or mepazine, an inhibitor of the MALT1 protease for which Regnase-1 is a substrate (Jeltsch et al., 2014). Western analysis also confirmed that Roquin-1 and Roquin-2 are not detectable after the respective KOs (Figure 1B). The *ZC3H12B* and *ZC3H12C* KOs could not be confirmed by Western analysis as the proteins are not sufficiently expressed within the parental HAP1 cells, and a KO of *ZC3H12D*, the remaining *ZC3H12* family member, was not made as it does not appear to be significantly expressed at the mRNA level in the HAP1 cells (Essletzbichler et al., 2014).

The KO of *ZC3H12A* resulted in decreased Tfr1 mRNA relative to the parental cells (Figure 1C), which is the opposite result expected for the KO of an enzyme catalyzing Tfr1 mRNA degradation. The decreased Tfr1 mRNA in the KO is not likely an artifact of an effect on the qPCR reference as the identical result was obtained using an independent qPCR reference (Figure S1A), and there was no indication that either reference was affected by the KO. The decreased Tfr1 mRNA in the KO also does not appear to result from increased expression of the other Regnase family members or Roquin (Figure S1B). In contrast to the effect of the *ZC3H12A* KO on Tfr1 mRNA, there was a threefold increase in the Cox-2 (*PTGS2*) mRNA (Figure 1D), which is a well-established Regnase-1 substrate (Mino et al., 2015). This result is consistent with the increased steady-state levels of *PTGS2* mRNA and other well-established Regnase-1 substrates that occur with the *ZC3H12A* KO/knockdown (KD) in other cell types (Matsushita et al., 2009; Mino et al., 2015). The result indicates that Regnase-1 is functional in the HAP1 cells and that there is not a redundant activity able to fully compensate for its loss.

Only the CRISPR KO of *RC3H1* or *RC3H2* resulted in the increased Tfr1 mRNA expected of a protein that induces or catalyzes Tfr1 mRNA degradation (Figure 1C). The *RC3H1* KO has the greatest effect, and the contribution of *RC3H2* becomes even more apparent when a *RC3H2* siRNA KD is performed in the context

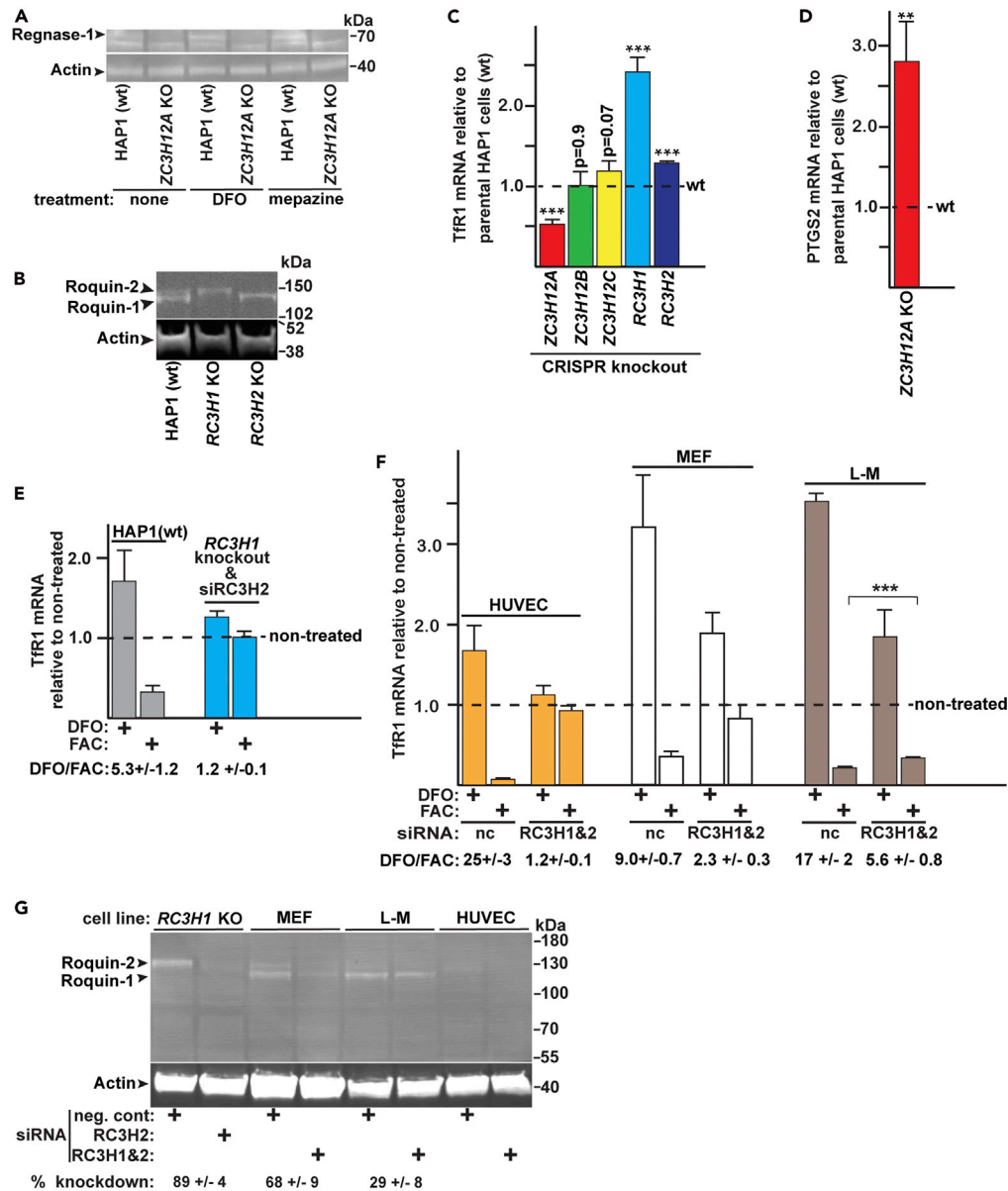


**Figure 1. Testing the relevance of ZC3H12A-C and RC3H1-2 to the steady-state level of TfR1 mRNA**

(A) Western analysis of Regnase-1 within the parental HAP1 (wt) and ZC3H12A KO, as described within the [transparent methods](#).

(B) Western analysis of the Roquin isoforms within the wt and RC3H1 and -2 KOs.

(C) Impact of the CRISPR KOs of the indicated Regnase and Roquin family members on the steady-state TfR1 mRNA level.

(D) The ZC3H12A KO increased the abundance of the PTGS2 mRNA, an established Regnase-1 substrate.

(E) The iron regulation of TfR1 mRNA abundance is eliminated by the Roquin KO/KD in HAP1 cells, as indicated by the ratio of the TfR1 mRNA abundance under iron deplete (DFO) and rich (FAC) conditions being close to one. Values are relative to the TfR1 mRNA in cells that had not been treated with either the DFO or FAC.

(F) The two Roquin isoforms can account for the majority of iron-regulated changes to TfR1 mRNA within the tested cell types, as indicated by the decreased DFO/FAC ratio in the presence of the KDs; nc = negative control siRNA.

(G) Western analysis of the Roquin KD in the different cell types. KD efficiencies were calculated from 3 to 5 biological replicates and are indicated below the representative blot. The expression of Roquin is too low in the HUVEC cells to unambiguously quantify the KD by the Western analysis. Cells where indicated were treated with FAC or DFO for 5 hr prior to harvesting. Data are the mean  $\pm$  standard error of the mean ( $n = 3-5$  biological replicates); \*\* $p < 0.01$ ; \*\*\* $p < 0.001$ . See also [Figure S1](#).

of the *RC3H1* CRISPR KO (Figure S1C). The increased TfR1 mRNA resulting from the *RC3H2* siRNA can be attributed to the KD of the intended target rather than to an off-target effect because the same siRNA does not impact the *RC3H2* CRISPR KO (Figure S1C). The result suggests that the two isoforms have partially redundant roles in mediating TfR1 mRNA instability, similar to other Roquin-regulated mRNAs (Leppke et al., 2013; Pratama et al., 2013; Vogel et al., 2013). The increased TfR1 mRNA within the Roquin KO/KD results in a 44% increase in the TfR1 protein relative to the wildtype cells (Figures S1D and S1E). This is especially significant given that the TfR1 is expected to be already elevated in the proliferating cells (O'Donnell et al., 2006; Sutherland et al., 1981).

The importance of the two Roquin isoforms to the iron regulation of the TfR1 mRNA was next tested in several cell types. TfR1 mRNA in HAP1 cells is approximately fivefold more abundant when grown in the presence of DFO than in the presence of ferric ammonium citrate (FAC), an iron source (Figure 1E). Strikingly, TfR1 mRNA fails to respond to changes in iron status with the combined *RC3H1* KO/*RC3H2* KD (DFO/FAC =  $1.2 \pm 0.1$ ). The attenuation of the DFO response by the KO/KD is consistent with IRP protection not being relevant when the degradation activity is eliminated, and the effect on the FAC response is consistent with no degradation activity even while IRP protection is minimized. This is similar to the increased TfR1 mRNA stability associated with mutations encompassing stem loops I, III, and V (Casey et al., 1989; Rupani and Connell, 2016). The results support the premise that the two Roquin isoforms can fully account for the iron-regulated change to TfR1 mRNA in HAP1 cells and argues strongly against a role for Regnase/MCPIP enzymes or other potential redundant activities therein. The importance of Roquin was also assessed in human umbilical vein endothelial cells (HUVECs), which are non-transformed primary cells. TfR1 mRNA is 25x more abundant under the DFO treatment than with FAC (Figure 1F), but this regulatory response was eliminated by the KD of the two Roquin isoforms (DFO/FAC =  $1.2 \pm 0.1$ ). The majority of the iron-regulated change to the TfR1 mRNA level is likewise blunted by Roquin KD in the two mouse cell types that were tested (Figure 1F): mouse embryonic fibroblasts (MEFs) and L-M cells, which is a fibroblast-like cell line used for the initial characterization of the TfR1 mRNA iron responsiveness (Casey et al., 1988b; Mullner and Kuhn, 1988). Although the effect of the KD is least impressive in the L-M cells (Figure 1F), the increase in TfR1 mRNA in response to DFO treatment is still blunted 1.9-fold by the KD; the decrease in response to FAC is blunted 1.6-fold; and the DFO/FAC ratio, which reflects the overall iron-regulated range, is blunted threefold. The efficiencies of the Roquin KDs at the mRNA level are similar in the four cell types (Figures S1F and S1G). However, there is a good correlation between the KD efficiency at the protein level and the impact of the KD on the iron responsiveness of the TfR1 mRNA level in the HAP1, L-M, and MEF cells. This is evident from a comparison of the percentage KD values indicated in Figure 1G with the DFO/FAC ratios that result from the KDs in Figures 1E and 1F. The expression of Roquin is too low in the HUVECs to unambiguously quantify the KD by the Western analysis (Figure 1G). Taken together, these results suggest that Roquin has a major role controlling cellular iron uptake.

### Roquin, but not Regnase-1, decreases TfR1 mRNA stability

The half-life of the TfR1 mRNA was measured in the context of the *ZC3H12A-C* and *RC3H1-2* CRISPR KOs to determine whether mRNA stability was impacted as opposed to there being indirect effects on transcription (Figure 2A). TfR1 mRNA in wildtype HAP1 cells decays with first order kinetics during the initial 5 hr of iron treatment (Figure 2B). The  $t_{1/2}$  of the TfR1 mRNA under these conditions is 1.1 hr (Table 1), which is comparable to the 1.5 hr observed in L-M cells (Mullner and Kuhn, 1988). The  $t_{1/2}$  was not significantly altered by the *ZC3H12A*, *ZC3H12B*, or *ZC3H12C* CRISPR KOs (Figure 2B and Table 1). Because the *ZC3H12A* KO does not have an impact on mRNA stability, it is likely that the decreased steady-state level observed in Figure 1C results from an indirect effect on TfR1 mRNA transcription. In contrast to the *ZC3H12* KOs, the  $t_{1/2}$  increased to 3 hr in the context of the *RC3H1* KO and to 8 hr in combination with the *RC3H2* siRNA KD. This is not significantly different than the 9.5 hr  $t_{1/2}$  measured during iron depletion and further indicates that the two Roquin isoforms, but not Regnase-1, can fully account for the TfR1 mRNA instability under iron-rich conditions (Table 1). Western analysis indicated that the protein level of Roquin-1 and Roquin-2 does not significantly change during the 5 hr period in which most of the degradation occurs, regardless of whether the cells are grown under iron-rich or deplete conditions (Figures 2C and 2D). We conclude that IRPs and Roquins are required iron-sensing and RNA destabilizing *trans*-acting factors, respectively, that control TfR1 mRNA accumulation and cellular iron uptake.

Roquin could potentially destabilize the TfR1 mRNA either directly through the recruitment of degradation enzymes or indirectly through the attenuation of IRP-mediated protection. The latter possibility is



**Table 1. TfR1 mRNA half-life in response to iron and the Regnase or Roquin isoform KO/KD**

Cell line/treatment	Slope ( $h^{-1}$ ) <sup>a</sup>	R <sup>2</sup>	TfR1 mRNA half-life (h)	95% confidence interval (h)
HAP1 (wt)/FAC	−0.64	0.96	1.1	0.9–1.3
HAP1 (wt)/DFO	−0.07	0.84	9.5	7.3–13.7
ZC3H12A KO/FAC	−0.66	0.95	1.1	0.9–1.3
ZC3H12B KO/FAC	−0.59	0.99	1.2	1.1–1.3
ZC3H12C KO/FAC	−0.57	0.99	1.2	1.1–1.3
RC3H1 KO & si(neg cont)/FAC	−0.21	0.96	3.3	2.9–3.8
RC3H1 KO & siRC3H2/FAC	−0.09	0.88	8.2	6.6–10.7

<sup>a</sup>Calculated from Figure 2B as described within the transparent methods.

mobility shift assay (EMSA). A shifted band that formed with both extracts and is more prominent during iron depletion is consistent with an IRE-IRP complex (Leibold and Munro, 1988; Rouault et al., 1988); the two human IRE-IRP complexes co-migrate in the EMSA (Guo et al., 1995; Henderson et al., 1993). This identity of the shifted band is further supported by competition with a 20-fold molar excess of unlabeled wild-type IRE but not with the deletion of two C nucleotides that are critical for IRP binding (Figures 2E and 2F). The IRE-IRP complex is equally iron responsive in both extracts suggesting that Roquin is not acting through the attenuation of IRP binding (Figure 2F). The result also suggests that there is a mechanism compensating for the increased iron importation that is expected from the elevated TfR1 expression within the Roquin KO/KD cells (Figures S1D and S1E).

### Roquin's specificity is consistent with the known requirements for iron-regulated TfR1 mRNA instability

The specificity of Roquin-1 was tested to determine whether it is consistent with the established structural features of the TfR1 mRNA previously identified as critical for TfR1 mRNA instability (loops I,III,V of Figure 3A; Rupani and Connell, 2016). A firefly luciferase reporter containing the minimized TfR1 mRNA instability region was used to assess the specificity, as it is a reliable surrogate of changes to mRNA abundance (Rupani and Connell, 2016). HAP1 cells were transfected in parallel with either the wildtype luciferase-TfR1 reporter or the same reporter containing mutations to the TfR1 hairpin loops (I,III,V). Mutation of the three loops individually or together increased firefly luciferase activity relative to the wildtype reporter when expressed in the parental HAP1 cells (Figure 3B). This is consistent with the loops being required for degradation, as was found for all tested cell types (Corral et al., 2019; Rupani and Connell, 2016). Whereas the ZC3H12A CRISPR KO had no effect on the relative luciferase activity of the mutated and wildtype reporters, the RC3H1 CRISPR KO decreased the relative impact of the loop mutations (I,III,V) by approximately half (Figure 3B). This decreased signal reflects increased stabilization of the reporter with the wildtype TfR1 3'-UTR relative to the reporter containing the mutated TfR1 3'-UTR. The combination of the RC3H1 KO with the RC3H2 KD completely nullified the difference in luciferase activity of the wildtype and mutated reporters. This effect is partially reversed by co-transfection with wildtype Roquin-1 (Figure 3B), but it is not with a mutation (K239A,R260A) that inhibits Roquin's function (Schlundt et al., 2014). The effect of the wildtype Roquin-1 co-transfection is probably underestimated as transfection under similar conditions with a  $\beta$ -galactosidase expressing plasmid indicated that only a small percentage (<10%) of the cells are transfected (transparent methods). Thus, we conclude that the two Roquin paralogs together account for the instability associated with the three hairpin loops.

### TfR1 mRNA instability under iron-rich conditions does not require ongoing translation

The impact of a block to translation on TfR1 mRNA abundance was tested to assess whether TfR1 mRNA instability was more consistent with a Regnase-1 or a Roquin-mediated reaction. The major characterized mechanism for Regnase-1-mediated mRNA instability requires active translation, whereas Roquin's mechanism does not (Mino et al., 2015, 2019). As a result, TfR1 mRNA abundance during iron treatment would be expected to increase when translation is inhibited if Regnase-1 has a major role. To test the importance of translation, a strong hairpin was inserted 4 nt upstream of the AUG start codon of the firefly luciferase-TfR1 reporter (Figure 3C). This hairpin has a predicted stability of  $-75$  kcal/mol and is known to effectively block translation (Doma and Parker, 2006). Translation inhibition was confirmed in the context of the luciferase-TfR1 reporter by the absence of detectable firefly luciferase activity (Figure 3D). However, the abundance of

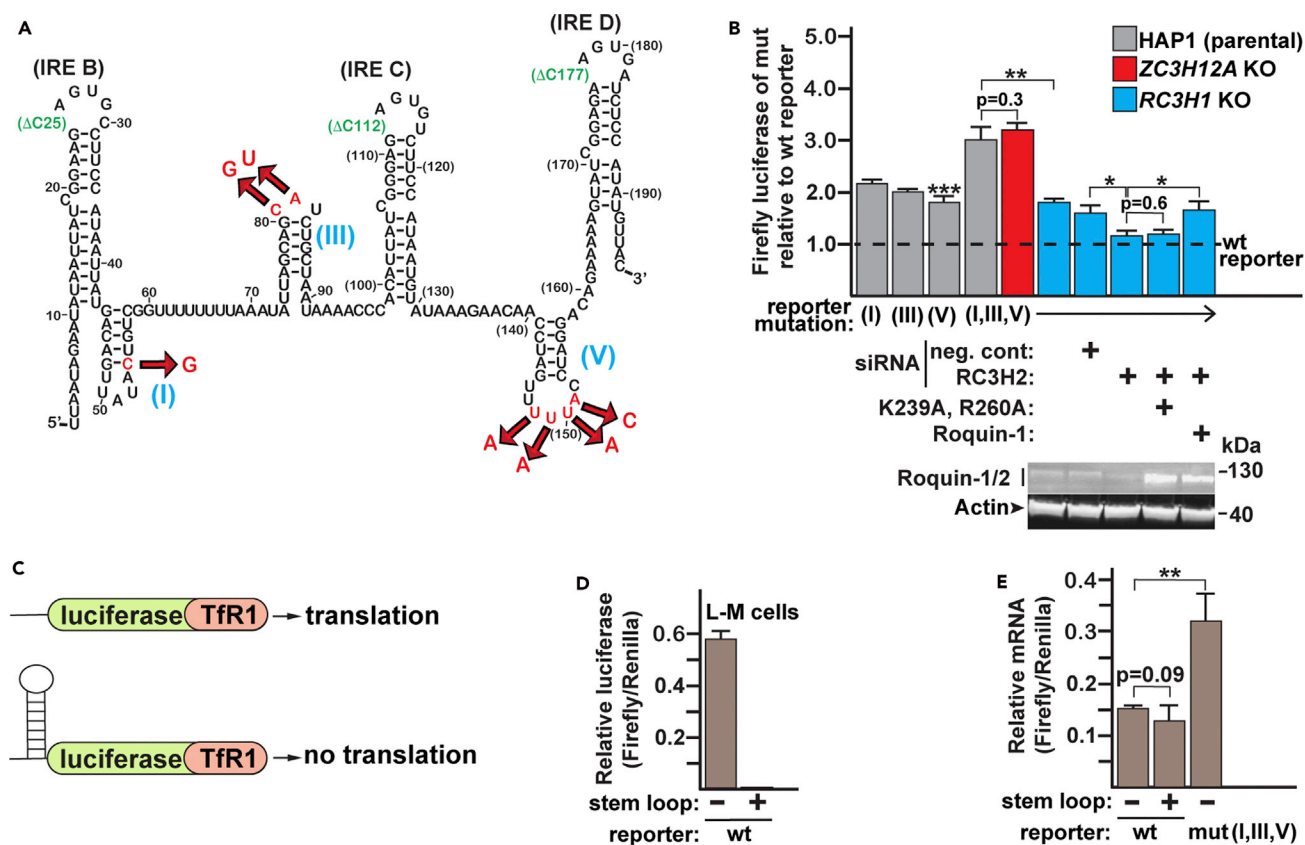


**Figure 3. Roquin's properties are consistent with the known requirements for iron-regulated TfR1 mRNA instability**

(A) Secondary structure of the minimized TfR1 3'-UTR instability sequence indicating mutations to the three hairpin loops (I,III,V) that inhibit degradation (red). Potential complications from changes to IRP binding and protection are avoided through single nucleotide deletions to the IRE loops (green). (B) Mutation of each non-IRE hairpin loop increased firefly luciferase activity relative to the wildtype (wt) reporter when expressed in HAP1 cells. KO/KD of Roquin, but not Regnase-1, negates the instability associated with the three TfR1 mRNA hairpin loops. This can be partially rescued by co-expression of Roquin-1 but not with a Roquin mutation (K239A, R260A) previously demonstrated to inhibit its activity. Western analysis of Roquin expression under each condition is indicated below the bar graph. (C) A strong hairpin was inserted 4 nt upstream of the AUG start codon of the firefly luciferase-TfR1 reporter. (D) The hairpin completely inhibits translation of the firefly luciferase-TfR1 reporter. Values are normalized to that of a *Renilla* luciferase activity encoded on the same plasmid as the firefly luciferase-TfR1 reporter. (E) Effect of the blockage to translation on the abundance of the firefly luciferase reporter mRNA. Mutation of the three essential hairpin loops (I,III,V) indicates the result expected if iron-regulated instability had been inhibited. The abundance of the firefly luciferase mRNA is relative to that of the *Renilla* luciferase mRNA. L-M cells were treated with 100  $\mu$ g/mL FAC for 14 hr prior to the assay. Data are the mean  $\pm$  SEM ( $n = 3$  biological replicates); \* $p < 0.02$ ; \*\* $p < 0.01$ ; \*\*\* $p < 0.001$ .

the firefly luciferase-TfR1 mRNA was not increased by the block to translation (Figure 3E), which should have occurred if instability were mediated by Regnase-1. In contrast, mutation of the three essential hairpin loops (I,III,V) increased the abundance of the reporter mRNA approximately twofold, indicating the result expected if iron-regulated instability had been inhibited. This result is consistent with a previous report that iron-regulated TfR1 mRNA instability occurs independently of translation (Posch et al., 1999). L-M cells were chosen for the assay because this cell type had the most iron regulation of the TfR1 mRNA remaining after the Roquin KD (Figure 1F). However, we conclude that the mechanism of TfR1 mRNA iron-regulated instability even in this cell type is not consistent with the major characterized mechanism of Regnase-1, but it is with that of Roquin.

## DISCUSSION

We demonstrated that the two Roquin paralogs mediate the majority of iron-regulated changes to the TfR1 mRNA in the four cell types tested, including both primary human and mouse cells (Figure 1). This role for Roquin is consistent with previous PAR-CLIP (Essig et al., 2018; Murakawa et al., 2015) and structural

conservation (Braun et al., 2018) studies that suggested an interaction with the Tfr1 mRNA. It could be speculated that the loss of the Tfr1 endonuclease activity would result in an iron overload condition such as hemochromatosis, as elevated Tfr1 expression in hepatocytes has the potential to decrease the HFE available to stimulate hepcidin expression (Fillebeen et al., 2019; Schmidt et al., 2008). However, studies of the impact of Roquin's KO on iron homeostasis have not yet been reported in animal models (Bertossi et al., 2011; Jeltsch et al., 2014; Schaefer et al., 2013), and there are only two *RC3H1* loss-of-function mutations that have been described in humans. The first is in a patient that is hemizygous for a large deletion in chromosome 1 that encompasses three genes including most of *RC3H1* (Kato et al., 2014). It results in clotting and autoimmunity disorders, but the diagnostic criteria that could be used to assess the presence of dysregulated iron metabolism were not reported. The second is a homozygous *RC3H1* nonsense mutation identified in a patient with elevated serum ferritin and hepatomegaly (Tavernier et al., 2019), which can be characteristics of iron overload. However, this attribution is complicated by a hyperinflammatory syndrome that has overlapping effects. A further complication is that the impact of the *RC3H1* mutations could be partially compensated by *RC3H2* as suggested by the effect of the *RC3H2* KD in the *RC3H1* CRISPR KO (Figures S1C and 2B). As a result, there is not yet any *in vivo* evidence to support Roquin's role in Tfr1 mRNA regulation.

The major evidence in support of a direct role for Regnase-1 as a mediator of Tfr1 mRNA degradation is the increased Tfr1 that is apparent in cells obtained from Regnase-1<sup>-/-</sup> null mice (Yoshinaga et al., 2017). However, an alternative explanation is that the increased Tfr1 is an indirect effect of the decreased transcription of *Cybrd1*, *Slc11a2*, and *Slc40a1*, which also occurs with the Regnase-1<sup>-/-</sup> null mice (Yoshinaga et al., 2017). In addition to these proteins being critical for duodenal iron absorption, *Slc11a2* (DMT1) is also important for the transport of iron out of the endosomes formed through the internalization of the transferrin-Tfr1 complex (reviewed in Yanatori and Kishi, 2019). As a result of decreased cytosolic iron, the Tfr1 mRNA could increase both from enhanced IRP protection and from the Tfr1 transcription that is likely stimulated by increased HIF- $\alpha$  activity (Nandal et al., 2011; Schwartz et al., 2019). An indirect effect would be consistent with the Regnase-1 KO having only an extremely modest impact on the endogenous Tfr1 mRNA stability when measured in the presence of actinomycin D (Figure 2A of Yoshinaga et al., 2017), and no significant impact when measured by the EU labeling reported here (Figure 2B). While the overexpression of Regnase-1 suggests that there is the potential for an interaction with Tfr1 mRNA (Yoshinaga et al., 2017), it is unclear whether this interaction would occur in the context of normal cellular protein and mRNA concentrations, which is a general limitation of overexpression-based studies (Prelich, 2012; Saito et al., 2016; Stuart et al., 2001). This complication could also explain an earlier report of Regnase-1 overexpression suppressing *Tnf* mRNA levels while Regnase-1 deficiency does not have an impact (Mino et al., 2015). The overexpression results, though, suggest that there is at least the possibility of Regnase-1 mediating Tfr1 mRNA degradation under conditions or in cell types that were not tested, especially if there is a high level of expression.

Tristetraprolin (TTP) is another CCCH type zinc finger protein that has been proposed to mediate the iron-regulated Tfr1 mRNA degradation (Bayeva et al., 2012). It binds to AU-rich elements (AREs) within the 3'-UTR of mRNAs and mediates degradation through the recruitment of deadenylation and decapping complexes, similar to Roquin. However, none of the proposed AREs are within the minimized Tfr1 mRNA sequence that supports efficient iron-regulated degradation in the tested cell types (Casey et al., 1989; Corral et al., 2019; Rupani and Connell, 2016). Whereas Roquin induces rapid Tfr1 mRNA degradation in response to excess iron (Figure 2B), TTP is more consistent with being a later stage response of mTOR-dependent changes to Tfr1 mRNA levels during iron depletion (Bayeva et al., 2012). The existence of at least two different Tfr1 mRNA degradation activities is supported by a rapid degradation activity that is present in the absence of TTP expression (Bayeva et al., 2012).

The minimal Tfr1 mRNA 3'-UTR sequence that induces efficient iron-regulated instability encompasses a ~200 nt region that contains three IREs and three non-IRE hairpin loops (I,III,V). The three non-IRE hairpin loops, which are essential for Tfr1 mRNA degradation, are highly similar to structures previously identified as interacting with Roquin. The reason for the apparent redundancy of the IREs and of the non-IRE hairpin loops has been unclear, but there are striking similarities to several other Roquin substrates which also contain multiple non-IRE hairpin loops (Essig et al., 2018). In these mRNAs, the redundancy is consistent with a model in which multiple simultaneous interactions determine the potency and robustness of the response. Roquin's interactions with mRNAs containing multiple non-IRE hairpin loops can directly inhibit translation, in addition to the induction of mRNA decay (Essig et al., 2018). As a result, graded changes to Tfr1 expression could occur through modulation

of both IRP protection and translation inhibition or mRNA decay, which could contribute to cell type- or situation-specific control of iron uptake. Further tuning of TfR1 expression is potentially achieved through changes to endocytic receptor trafficking (Cao et al., 2016), microRNAs (Babu and Muckenthaler, 2019), transcription, or TTP. In summary, we have shown that Roquin is a major mediator of iron-regulated TfR1 mRNA degradation within each of the four cell types that were tested, suggesting that it could also be relevant to several pathological conditions associated with either dysregulation of iron metabolism or TfR1 signaling.

### Limitations of the study

The relative importance of Roquin to TfR1 mRNA stability is most likely underestimated in some of the cell types used in this study as there is significant variability in the amount of Roquin remaining after the KD (Figure 1G). As already indicated, we cannot exclude the possibility that alternative mechanisms of TfR1 mRNA degradation are more prominent in cell types that were not tested. However, potential alternative activities need to satisfy several criteria: inhibition of the activity should both attenuate iron regulation of the endogenous TfR1 mRNA and significantly increase the TfR1 mRNA half-life and the specificity of the activity needs to be consistent with the established TfR1 mRNA structural features and other obligatory requirements of iron-regulated degradation. Although this study firmly establishes Roquin as a major mediator of TfR1 mRNA degradation within the cell types that were tested, there have not yet been studies demonstrating the significance of the protein to the organismal regulation of TfR1 and overall iron homeostasis.

### Resource availability

#### Lead contact

Further information and requests for resources and reagents should be directed to and will be fulfilled by the lead contact, Greg Connell ([conne018@umn.edu](mailto:conne018@umn.edu)).

#### Materials availability

All unique/stable reagents generated in this study are available from the lead contact without restriction.

#### Data and code availability

This study did not generate/analyze data sets/code.

## METHODS

All methods can be found in the accompanying [transparent methods supplemental file](#).

## SUPPLEMENTAL INFORMATION

Supplemental information can be found online at <https://doi.org/10.1016/j.isci.2021.102360>.

## ACKNOWLEDGMENTS

We thank O Takeuchi (Kyoto University, Japan) for a Regnase-1 expression plasmid. This work was supported in part by a University of Minnesota Multicultural Summer Research Opportunities Program (MSROP) award to V.M.C., an Undergraduate Research Opportunities Program (UROP) award to E.R.S., and a Grant-in-Aid from the Office of the Vice President for Research to G.J.C. We also acknowledge the University of Minnesota Imaging Centers for use of the phosphor scanner.

## AUTHOR CONTRIBUTIONS

V.M.C., E.R.S., and G.J.C. contributed to the conduction and design of the experiments as well as the writing of the paper. R.S.E. contributed to the design of the experiments and writing of the paper.

## DECLARATION OF INTERESTS

The authors declare no competing interests.

Received: May 6, 2020

Revised: September 18, 2020

Accepted: March 23, 2021

Published: April 23, 2021

**REFERENCES**

- Babu, K.R., and Muckenthaler, M.U. (2019). miR-148a regulates expression of the transferrin receptor 1 in hepatocellular carcinoma. *Sci. Rep.* **9**, 1518.
- Barrientos, T., Laothamatas, I., Koves, T.R., Soderblom, E.J., Bryan, M., Moseley, M.A., Muoio, D.M., and Andrews, N.C. (2015). Metabolic catastrophe in mice lacking transferrin receptor in muscle. *EBioMedicine* **2**, 1705–1717.
- Bayeva, M., Khechaduri, A., Puig, S., Chang, H.C., Patial, S., Blackshear, P.J., and Ardehali, H. (2012). mTOR regulates cellular iron homeostasis through tristetraprolin. *Cell Metab.* **16**, 645–657.
- Bertossi, A., Aichinger, M., Sansonetti, P., Lech, M., Neff, F., Pal, M., Wunderlich, F.T., Anders, H.J., Klein, L., and Schmidt-Supprian, M. (2011). Loss of Roquin induces early death and immune deregulation but not autoimmunity. *J. Exp. Med.* **208**, 1749–1756.
- Braun, J., Fischer, S., Xu, Z.Z., Sun, H., Ghoneim, D.H., Gimbel, A.T., Plessmann, U., Urlaub, H., Mathews, D.H., and Weigand, J.E. (2018). Identification of new high affinity targets for Roquin based on structural conservation. *Nucleic Acids Res.* **46**, 12109–12125.
- Cao, H., Schroeder, B., Chen, J., Schott, M.B., and McNiven, M.A. (2016). The endocytic fate of the transferrin receptor is regulated by c-Abl kinase. *J. Biol. Chem.* **291**, 16424–16437.
- Casey, J.L., Di Jeso, B., Rao, K., Klausner, R.D., and Harford, J.B. (1988a). Two genetic loci participate in the regulation by iron of the gene for the human transferrin receptor. *Proc. Natl. Acad. Sci. U S A* **85**, 1787–1791.
- Casey, J.L., Hentze, M.W., Koeller, D.M., Caughman, S.W., Rouault, T.A., Klausner, R.D., and Harford, J.B. (1988b). Iron-responsive elements: regulatory RNA sequences that control mRNA levels and translation. *Science* **240**, 924–928.
- Casey, J.L., Koeller, D.M., Ramin, V.C., Klausner, R.D., and Harford, J.B. (1989). Iron regulation of transferrin receptor mRNA levels requires iron-responsive elements and a rapid turnover determinant in the 3' untranslated region of the mRNA. *EMBO J.* **8**, 3693–3699.
- Chen, A.C., Donovan, A., Ned-Sykes, R., and Andrews, N.C. (2015). Noncanonical role of transferrin receptor 1 is essential for intestinal homeostasis. *Proc. Natl. Acad. Sci. U S A* **112**, 11714–11719.
- Corral, V.M., Schultz, E.R., and Connell, G.J. (2019). Neither miR-7-5p nor miR-141-3p is a major mediator of iron-responsive transferrin receptor-1 mRNA degradation. *RNA* **25**, 1407–1415.
- Coulon, S., Dussiot, M., Grapton, D., Maciel, T.T., Wang, P.H., Callens, C., Tiwari, M.K., Agarwal, S., Fricot, A., Vandekerckhove, J., et al. (2011). Polymeric IgA1 controls erythroblast proliferation and accelerates erythropoiesis recovery in anemia. *Nat. Med.* **17**, 1456–1465.
- Doma, M.K., and Parker, R. (2006). Endonucleolytic cleavage of eukaryotic mRNAs with stalls in translation elongation. *Nature* **440**, 561–564.
- Essig, K., Kronbeck, N., Guimaraes, J.C., Lohs, C., Schlundt, A., Hoffmann, A., Behrens, G., Brenner, S., Kowalska, J., Lopez-Rodriguez, C., et al. (2018). Roquin targets mRNAs in a 3'-UTR-specific manner by different modes of regulation. *Nat. Commun.* **9**, 3810.
- Esslitzbichler, P., Konopka, T., Santoro, F., Chen, D., Gapp, B.V., Kralovics, R., Brummelkamp, T.R., Nijman, S.M.B., and Burckstummer, T. (2014). Megabase-scale deletion using CRISPR/Cas9 to generate a fully haploid human cell line. *Genome Res.* **24**, 2059–2065.
- Fillebeen, C., Charlebois, E., Wagner, J., Katsarou, A., Mui, J., Vali, H., Garcia-Santos, D., Ponka, P., Presley, J., and Pantopoulos, K. (2019). Transferrin receptor 1 controls systemic iron homeostasis by fine-tuning hepcidin expression to hepatocellular iron load. *Blood* **133**, 344–355.
- Galaris, D., Barbouti, A., and Pantopoulos, K. (2019). Iron homeostasis and oxidative stress: an intimate relationship. *Biochim* **1866**, 118535.
- Ghosh, M.C., Zhang, D.-L., and Rouault, T.A. (2015). Iron misregulation and neurodegenerative disease in mouse models that lack iron regulatory proteins. *Neurobiol. Dis.* **81**, 66–75.
- Glasmacher, E., Hoefig, K.P., Vogel, K.U., Rath, N., Du, L., Wolf, C., Kremmer, E., Wang, X., and Heissmeyer, V. (2010). Roquin binds inducible costimulatory mRNA and effectors of mRNA decay to induce microRNA-independent post-transcriptional repression. *Nat. Immunol.* **11**, 725–733.
- Guo, B., Brown, F.M., Phillips, J.D., Yu, Y., and Leibold, E.A. (1995). Characterization and expression of iron regulatory protein 2 (IRP2). Presence of multiple IRP2 transcripts regulated by intracellular iron levels. *J. Biol. Chem.* **270**, 16529–16535.
- Hao, S., Li, H., Sun, X., Li, J., and Li, K. (2015). An unusual case of iron deficiency anemia is associated with extremely low level of transferrin receptor. *Int. J. Clin. Exp. Pathol.* **8**, 8613–8618.
- Henderson, B.R., Seiser, C., and Kuhn, L.C. (1993). Characterization of a second RNA-binding protein in rodents with specificity for iron-responsive elements. *J. Biol. Chem.* **268**, 27327–27334.
- Jabara, H.H., Boyden, S.E., Chou, J., Ramesh, N., Massaad, M.J., Benson, H., Bainter, W., Fraulino, D., Rahimov, F., Sieff, C., et al. (2016). A missense mutation in TFRC, encoding transferrin receptor 1, causes combined immunodeficiency. *Nat. Genet.* **48**, 74–78.
- Janowski, R., Heinz, G.A., Schlundt, A., Wommelsdorf, N., Brenner, S., Gruber, A.R., Blank, M., Buch, T., Buhmann, R., Zavolan, M., et al. (2016). Roquin recognizes a non-canonical hexaloop structure in the 3'-UTR of Ox40. *Nat. Commun.* **7**, 11032.
- Jeltsch, K.M., Hu, D., Brenner, S., Zoller, J., Heinz, G.A., Nagel, D., Vogel, K.U., Rehage, N., Warth, S.C., Edelmann, S.L., et al. (2014). Cleavage of roquin and regnase-1 by the paracaspase MALT1 releases their cooperatively repressed targets to promote T(H)17 differentiation. *Nat. Immunol.* **15**, 1079–1089.
- Kato, I., Takagi, Y., Ando, Y., Nakamura, Y., Murata, M., Takagi, A., Murate, T., Matsushita, T., Nakashima, T., and Kojima, T. (2014). A complex genomic abnormality found in a patient with antithrombin deficiency and autoimmune disease-like symptoms. *Int. J. Hematol.* **100**, 200–205.
- Larrick, J.W., and Hyman, E.S. (1984). Acquired iron-deficiency anemia caused by an antibody against the transferrin receptor. *N. Engl. J. Med.* **311**, 214–218.
- Leibold, E.A., and Munro, H.N. (1988). Cytoplasmic protein binds in vitro to a highly conserved sequence in the 5' untranslated region of ferritin heavy- and light-subunit mRNAs. *Proc. Natl. Acad. Sci. U S A* **85**, 2171–2175.
- Leppek, K., Schott, J., Reitter, S., Poetz, F., Hammond, M.C., and Stoecklin, G. (2013). Roquin promotes constitutive mRNA decay via a conserved class of stem-loop recognition motifs. *Cell* **153**, 869–881.
- Levy, J.E., Jin, O., Fujiwara, Y., Kuo, F., and Andrews, N.C. (1999). Transferrin receptor is necessary for development of erythrocytes and the nervous system. *Nat. Genet.* **21**, 396–399.
- Li, H., Choesang, T., Bao, W., Chen, H., Feola, M., Garcia-Santos, D., Li, J., Sun, S., Follenzi, A., Pham, P., et al. (2017). Decreasing TfR1 expression reverses anemia and hepcidin suppression in beta-thalassemic mice. *Blood* **129**, 1514–1526.
- Liang, J., Wang, J., Azfer, A., Song, W., Tromp, G., Kolattukudy, P.E., and Fu, M. (2008). A novel CCH-zinc finger protein family regulates proinflammatory activation of macrophages. *J. Biol. Chem.* **283**, 6337–6346.
- Lok, C.N., and Ponka, P. (1999). Identification of a hypoxia response element in the transferrin receptor gene. *J. Biol. Chem.* **274**, 24147–24152.
- Matak, P., Matak, A., Moustafa, S., Aryal, D.K., Benner, E.J., Wetsel, W., and Andrews, N.C. (2016). Disrupted iron homeostasis causes dopaminergic neurodegeneration in mice. *Proc. Natl. Acad. Sci. U S A* **113**, 3428–3435.
- Matsushita, K., Takeuchi, O., Standley, D.M., Kumagai, Y., Kawagoe, T., Miyake, T., Satoh, T., Kato, H., Tsujimura, T., Nakamura, H., et al. (2009). Zc3h12a is an RNase essential for controlling immune responses by regulating mRNA decay. *Nature* **458**, 1185–1190.
- Mino, T., Iwai, N., Endo, M., Inoue, K., Akaki, K., Hia, F., Uehata, T., Emura, T., Hidaka, K., Suzuki, Y., et al. (2019). Translation-dependent unwinding of stem-loops by UPF1 licenses Regnase-1 to degrade inflammatory mRNAs. *Nucleic Acids Res.* **47**, 8838–8859.
- Mino, T., Murakawa, Y., Fukao, A., Vandenbon, A., Wessels, H.-H., Ori, D., Uehata, T., Tarte, S., Akira, S., Suzuki, Y., et al. (2015). Regnase-1 and Roquin regulate a common element in inflammatory mRNAs by spatiotemporally distinct mechanisms. *Cell* **161**, 1058–1073.

- Mullner, E.W., and Kuhn, L.C. (1988). A stem-loop in the 3' untranslated region mediates iron-dependent regulation of transferrin receptor mRNA stability in the cytoplasm. *Cell* 53, 815–825.
- Murakawa, Y., Hinz, M., Mothes, J., Schuetz, A., Uhl, M., Wyler, E., Yasuda, T., Mastrobuoni, G., Friedel, C.C., Dolken, L., et al. (2015). RC3H1 post-transcriptionally regulates A20 mRNA and modulates the activity of the IKK/NF-kappaB pathway. *Nat. Commun.* 6, 7367.
- Nakamura, T., Naguro, I., and Ichijo, H. (2019). Iron homeostasis and iron-regulated ROS in cell death, senescence and human diseases. *Biochim. Biophys. Acta* 1863, 1398–1409.
- Nandal, A., Ruiz, J.C., Subramanian, P., Ghimire-Rijal, S., Sinnamon, R.A., Stemmler, T.L., Bruick, R.K., and Philpott, C.C. (2011). Activation of the HIF prolyl hydroxylase by the iron chaperones PCBP1 and PCBP2. *Cell Metab.* 14, 647–657.
- O'Donnell, K.A., Yu, D., Zeller, K.I., Kim, J.W., Racke, F., Thomas-Tikhonenko, A., and Dang, C.V. (2006). Activation of transferrin receptor 1 by c-Myc enhances cellular proliferation and tumorigenesis. *Mol. Cell Biol.* 26, 2373–2386.
- Owen, D., and Kuhn, L.C. (1987). Noncoding 3' sequences of the transferrin receptor gene are required for mRNA regulation by iron. *EMBO J.* 6, 1287–1293.
- Pham, D.H., Powell, J.A., Gliddon, B.L., Moretti, P.A.B., Tsykin, A., Van der Hoek, M., Kenyon, R., Goodall, G.J., and Pitson, S.M. (2014). Enhanced expression of transferrin receptor 1 contributes to oncogenic signalling by sphingosine kinase 1. *Oncogene* 33, 5559–5568.
- Posch, M., Sutterluety, H., Skern, T., and Seiser, C. (1999). Characterization of the translation-dependent step during iron-regulated decay of transferrin receptor mRNA. *J. Biol. Chem.* 274, 16611–16618.
- Pratama, A., Ramiscal, R.R., Silva, D.G., Das, S.K., Athanasopoulos, V., Fitch, J., Botelho, N.K., Chang, P.-P., Hu, X., Hogan, J.J., et al. (2013). Roquin-2 shares functions with its paralog Roquin-1 in the repression of mRNAs controlling T follicular helper cells and systemic inflammation. *Immunity* 38, 669–680.
- Prelich, G. (2012). Gene overexpression: uses, mechanisms, and interpretation. *Genetics* 190, 841–854.
- Rehage, N., Davydova, E., Conrad, C., Behrens, G., Maiser, A., Stehlein, J.E., Brenner, S., Klein, J., Jeridi, A., Hoffmann, A., et al. (2018). Binding of NUFIP2 to Roquin promotes recognition and regulation of ICOS mRNA. *Nat. Commun.* 9, 299.
- Rouault, T.A., Hentze, M.W., Caughman, S.W., Harford, J.B., and Klausner, R.D. (1988). Binding of a cytosolic protein to the iron-responsive element of human ferritin messenger RNA. *Science* 241, 1207–1210.
- Rupani, D.N., and Connell, G.J. (2016). Transferrin receptor mRNA interactions contributing to iron homeostasis. *RNA* 22, 1271–1282.
- Saito, T., Matsuba, Y., Yamazaki, N., Hashimoto, S., and Saido, T.C. (2016). Calpain activation in Alzheimer's model mice is an artifact of APP and Presenilin overexpression. *J. Neurosci.* 36, 9933–9936.
- Salmeron, A., Borroto, A., Fresno, M., Crumpton, M.J., Ley, S.C., and Alarcon, B. (1995). Transferrin receptor induces tyrosine phosphorylation in T cells and is physically associated with the TCR zeta-chain. *J. Immunol.* 154, 1675–1683.
- Santos, M.C.F.D., Anderson, C.P., Neschen, S., Zumbrennen-Bullough, K.B., Romney, S.J., Kahle-Stephan, M., Rathkolb, B., Gailus-Durner, V., Fuchs, H., Wolf, E., et al. (2020). Irf2 regulates insulin production through iron-mediated Cdkal1-catalyzed tRNA modification. *Nat. Commun.* 11, 296.
- Schaefer, J.S., Montufar-Solis, D., Nakra, N., Vigneswaran, N., and Klein, J.R. (2013). Small intestine inflammation in Roquin-mutant and Roquin-deficient mice. *PLoS One* 8, e56436.
- Schlundt, A., Heinz, G.A., Janowski, R., Geerlof, A., Stehle, R., Heissmeyer, V., Niessing, D., and Sattler, M. (2014). Structural basis for RNA recognition in roquin-mediated post-transcriptional gene regulation. *Nat. Struct. Mol. Biol.* 21, 671–678.
- Schmidt, P.J., Toran, P.T., Giannetti, A.M., Bjorkman, P.J., and Andrews, N.C. (2008). The transferrin receptor modulates Hfe-dependent regulation of hepcidin expression. *Cell Metab.* 7, 205–214.
- Schwartz, A.J., Converso-Baran, K., Michele, D.E., and Shah, Y.M. (2019). A genetic mouse model of severe iron deficiency anemia reveals tissue-specific transcriptional stress responses and cardiac remodeling. *J. Biol. Chem.* 294, 14991–15002.
- Senyilmaz, D., Virtue, S., Xu, X., Tan, C.Y., Griffin, J.L., Miller, A.K., Vidal-Puig, A., and Teleman, A.A. (2015). Regulation of mitochondrial morphology and function by stearoylation of TFR1. *Nature* 525, 124–128.
- Shen, Y., Li, X., Dong, D., Zhang, B., Xue, Y., and Shang, P. (2018). Transferrin receptor 1 in cancer: a new sight for cancer therapy. *Am. J. Cancer Res.* 8, 916–931.
- Stuart, J.A., Harper, J.A., Brindle, K.M., Jakobsons, M.B., and Brand, M.D. (2001). A mitochondrial uncoupling artifact can be caused by expression of uncoupling protein 1 in yeast. *Biochem. J.* 356, 779–789.
- Sutherland, R., Delia, D., Schneider, C., Newman, R., Kemshead, J., and Greaves, M. (1981). Ubiquitous cell-surface glycoprotein on tumor cells is proliferation-associated receptor for transferrin. *Proc. Natl. Acad. Sci. U S A* 78, 4515–4519.
- Tacchini, L., Bianchi, L., Bernelli-Zazzera, A., and Cairo, G. (1999). Transferrin receptor induction by hypoxia. HIF-1-mediated transcriptional activation and cell-specific post-transcriptional regulation. *J. Biol. Chem.* 274, 24142–24146.
- Tan, D., Zhou, M., Kiledjian, M., and Tong, L. (2014). The ROQ domain of Roquin recognizes mRNA constitutive-decay element and double-stranded RNA. *Nat. Struct. Mol. Biol.* 21, 679–685.
- Tavernier, S.J., Athanasopoulos, V., Verloo, P., Behrens, G., Staal, J., Bogaert, D.J., Naesens, L., De Bruyne, M., Van Gassen, S., Parthoens, E., et al. (2019). A human immune dysregulation syndrome characterized by severe hyperinflammation with a homozygous nonsense Roquin-1 mutation. *Nat. Commun.* 10, 4779.
- Vinuesa, C.G., Cook, M.C., Angelucci, C., Athanasopoulos, V., Rui, L., Hill, K.M., Yu, D., Domaschensz, H., Whittle, B., Lambe, T., et al. (2005). A RING-type ubiquitin ligase family member required to repress follicular helper T cells and autoimmunity. *Nature* 435, 452–458.
- Vogel, K.U., Edelmann, S.L., Jeltsch, K.M., Bertossi, A., Heger, K., Heinz, G.A., Zoller, J., Warth, S.C., Hoefig, K.P., Lohs, C., et al. (2013). Roquin paralogs 1 and 2 redundantly repress the Icos and Ox40 costimulator mRNAs and control follicular helper T cell differentiation. *Immunity* 38, 655–668.
- Wawro, M., Wawro, K., Kochan, J., Solecka, A., Sowinska, W., Lichawska-Cieslar, A., Jura, J., and Kasza, A. (2019). ZC3H12B/MCPIP2, a new active member of the ZC3H12 family. *RNA* 25, 840–856.
- Xu, W., Barrientos, T., Mao, L., Rockman, H.A., Sauve, A.A., and Andrews, N.C. (2015). Lethal cardiomyopathy in mice lacking transferrin receptor in the heart. *Cell Rep.* 13, 533–545.
- Yanatori, I., and Kishi, F. (2019). DMT1 and iron transport. *Free Radic. Biol. Med.* 133, 55–63.
- Yokogawa, M., Tsushima, T., Noda, N.N., Kumeta, H., Enokizono, Y., Yamashita, K., Standley, D.M., Takeuchi, O., Akira, S., and Inagaki, F. (2016). Structural basis for the regulation of enzymatic activity of Regnase-1 by domain-domain interactions. *Sci. Rep.* 6, 22324.
- Yoshinaga, M., Nakatsuka, Y., Vandebon, A., Ori, D., Uehata, T., Tsujimura, T., Suzuki, Y., Mino, T., and Takeuchi, O. (2017). Regnase-1 maintains iron homeostasis via the degradation of transferrin receptor 1 and prolyl-hydroxylase-domain-containing protein 3 mRNAs. *Cell Rep.* 19, 1614–1630.
- Yoshinaga, M., and Takeuchi, O. (2019). Post-transcriptional control of immune responses and its potential application. *Clin. Transl. Immunol.* 8 (6), e1063.

**iScience, Volume 24**

**Supplemental information**

**Roquin is a major mediator  
of iron-regulated changes to transferrin  
receptor-1 mRNA stability**

**Victor M. Corral, Eric R. Schultz, Richard S. Eisenstein, and Gregory J. Connell**

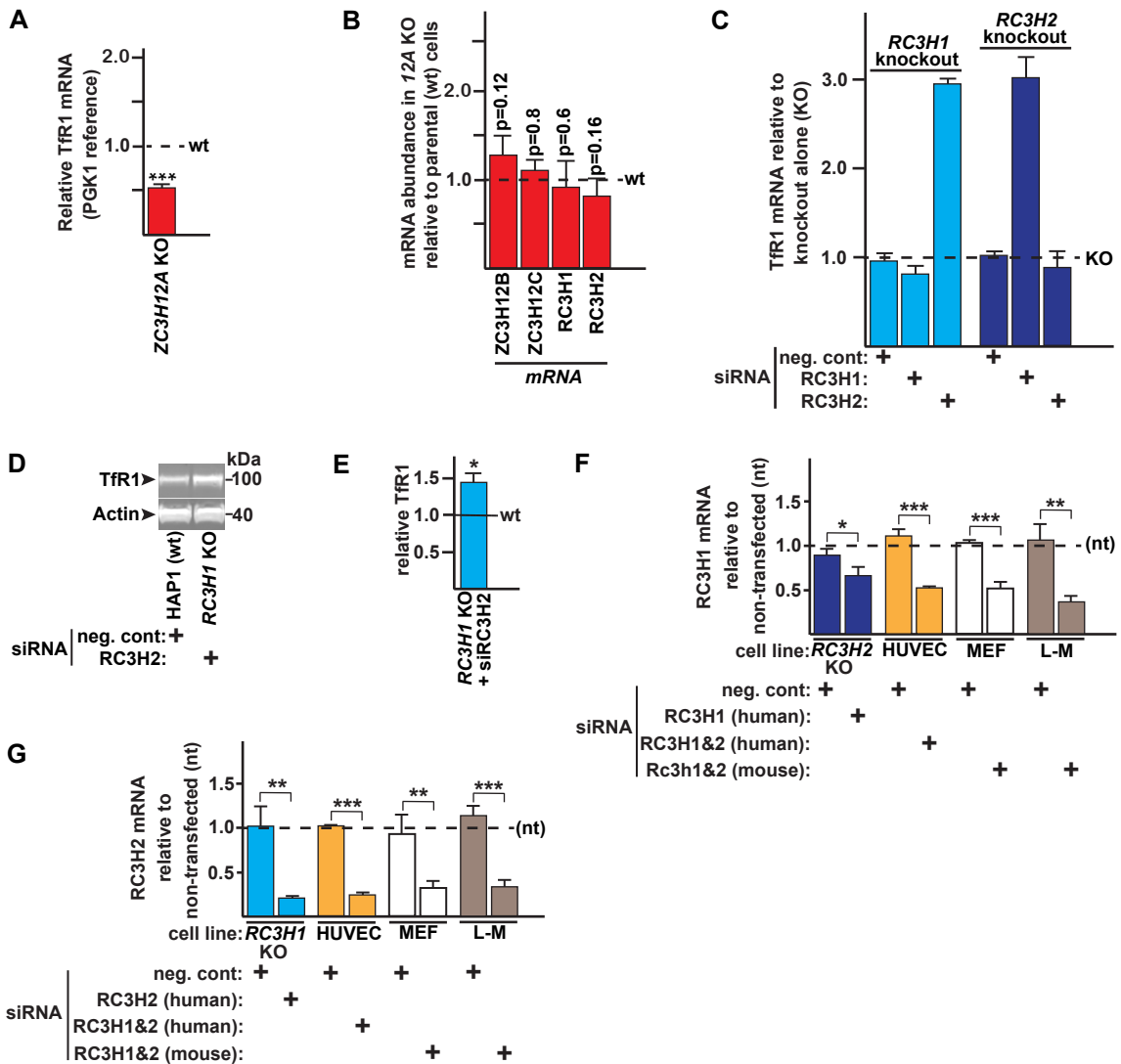


**Figure S1. Testing the relevance of ZC3H12A-C and RC3H1 and -2 to the steady-state TfR1 mRNA level, related to Figure 1.**

(A) Quantification of the TfR1 mRNA in the ZC3H12A KO using PGK1 as the RT-qPCR reference. (B) The change in abundance of the indicated mRNAs in the ZC3H12A KO cells relative to the parental cells (wt). ZC3H12D was not included in the analysis as it is not sufficiently expressed in the HAP1 cells under either condition. (C) The two Roquin paralogs are partially redundant. Neither siRNA increases the TfR1 mRNA in the context of a CRISPR KO of the intended target. (D) Western analysis of the impact of the Roquin KO/KD on the TfR1 protein. (E) Quantification of the Western analysis in (D). (F) Efficiency of the siRNA KD of RC3H1 mRNA in the cell types used for the study. (G) Efficiency of the siRNA KD of RC3H2 mRNA. Data are the mean +/- SEM (n=3 biological replicates); \*p<0.03; \*\*p<0.01; \*\*\*p<0.001.

**Table S1** Key Resources, related to Figures 1-3

REAGENT or RESOURCE	SOURCE	IDENTIFIER
<b>Antibodies</b>		
Anti-Actin (I-19) - goat polyclonal	Santa Cruz Bio	Cat # sc1616
Anti-Flag (M2) – mouse monoclonal	Millipore Sigma	Cat # F1804
Anti-Regnase-1 - rabbit polyclonal	Proteintech	Cat # 25009.1
Anti-Roquin-1/2 (3F12) - rat monoclonal	Millipore-Sigma	Cat # MABF288
Anti-TfR1 (H68.4) - mouse monoclonal	Thermo Scientific	Cat # 13-6800
Donkey anti-goat with IR linked dye (800CW)	Li-Cor	Cat # 925-32214
Donkey anti-Rabbit with IR linked dye (800 CW)	Li-Cor	Cat # 925-32213
Goat anti-mouse with IR linked dye (800 CW)	Li-Cor	Cat # 925-32210
Goat anti-rat with IR linked dye (800 CW)	Li-Cor	Cat # 925-32219
<b>Cell Lines</b>		
Human: HAP1 parental cells	Horizon Discovery	C631
Human: HAP1 <i>RC3H1</i> knockout cells	Horizon Discovery	HZGHC007428c012
Human: HAP1 <i>RC3H2</i> knockout cells	Horizon Discovery	HZGHC007421c010
Human: HAP1 <i>ZC3H12A</i> knockout cells	Horizon Discovery	HZGHC006348c002
Human: HAP1 <i>ZC3H12B</i> knockout cells	Horizon Discovery	HZGHC007320c004
Human: HAP1 <i>ZC3H12C</i> knockout cells	Horizon Discovery	HZGHC007322c007
Human: HUVEC cells	Lonza	C2517A
Mouse: MEF cells	Millipore-Sigma	PMEF-CFL-C
Mouse: L-M (TK-) cells	ATCC	CCL-1.3
<b>Oligonucleotides</b>		
Oligonucleotides for PCR	IDT (See Table S2)	N/A
siRNA targeting RC3H1 (human): GAUCGAGAGUUACUAUCC	Thermo Scientific	Cat# 4427037 (s45244)
siRNA targeting Rc3h1 (mouse): GGUUCUGCAUUGUCUCGGA	Thermo Scientific	Cat# 4390771 (s117591)
siRNA targeting RC3H2 (human): CAAGGACUCAGAUACCCUU	Thermo Scientific	Cat# 4427037 (s29171)
siRNA targeting Rc3h2 (mouse): CCAGAAUCAUUUGCAAAGA	Thermo Scientific	Cat# 4390771 (s232965)
Silencer Select Negative Control #1 siRNA	Thermo Scientific	Cat# 4390843
Silencer Select Negative Control #2 siRNA	Thermo Scientific	Cat# 4390846
<b>Recombinant DNA</b>		
Luciferase-TfR1 parental in pMIRGLO (OPT1)	(Rupani and Connell, 2016)	N/A
Luciferase-TfR1 mutation loop (I)	(Corral et al., 2019)	N/A
Luciferase-TfR1 mutation loop (III)	(Corral et al., 2019)	N/A
Luciferase-TfR1 mutation loop (V)	(Corral et al., 2019)	N/A
Luciferase-TfR1 mutation loop (I,III,V)	(Rupani and Connell, 2016)	N/A
Luciferase-TfR1 parental (OPT1) + 5' hairpin	This work	N/A
RC3H1 (human) in pSF-SMV-NEO-NH2-3xFlag	This work	N/A
K239A, R260A (RC3H1) in pSF-SMV-NEO-NH2-3xFlag	This work	N/A

<b>Software</b>		
Codon optimization	Gensmart Codon Optimization	<a href="https://www.genscript.com/">https://www.genscript.com/</a>
Curve fitting	R version 3.6.1	<a href="https://www.r-project.org/">https://www.r-project.org/</a>
Primer Blast (for design of qPCR primers)	N/A	<a href="https://www.ncbi.nlm.nih.gov/tools/primer-blast/index.cgi?LINK_LOC=BlastHome">https://www.ncbi.nlm.nih.gov/tools/primer-blast/index.cgi?LINK_LOC=BlastHome</a>
qPCR analysis	Thermo Scientific StepOne software V2.3	<a href="https://www.thermofisher.com/us/en/home/technical-resources/software-downloads/StepOne-and-StepOnePlus-Real-Time-PCR-System.html">https://www.thermofisher.com/us/en/home/technical-resources/software-downloads/StepOne-and-StepOnePlus-Real-Time-PCR-System.html</a>
T test calculator for 2 independent means	N/A	<a href="https://www.socscistatistics.com/">https://www.socscistatistics.com/</a>
Western and EMSA quantitation	Image Studio version 5.2.5 (Li-Cor)	N/A

**Table S2** Oligonucleotides used for the qPCR and to validate the HAP1 cell knockouts, related to Figures 1-3

<b>Amplicon</b>	<b>NCBI reference</b>	<b>Location</b>	<b>PCR primers</b>
<b>qPCR</b>			
Firefly luciferase (pmirGLO)	FJ376737	7117-7188	AACCATGACCGAGAAGGAGATC CCACCGCGCAGCTTCTT
PGK1 human	NM_000291.4	1095-1179	TGTGTGGAATGGTCCTGTGG GGCTTTCACCACCTCATCCA
PTGS2 human	NM_000963.4	4020-4095	GGGATCTGTGGATGCTTCGT AACCCACAGTGCTTGACACA
Renilla luciferase (pmirGLO)	FJ376737	2227-2293	ATGCGGCGGCTGCATA GATGCGATGTTTCGCTTGGT
TfR1 human	NM_003234.3	4442-4528	AGAGTCCCCTGAAGGTCTGACA CTCACGGAGCTTCGAACTTATTC
TfR1 mouse	NM_011638.4	4382-4460	GTCACTAGGCTCTCAGGGTCTTG AAACAACCTCAGTGAGGCTCAAATAA
RPL4 human	NM_000968.4	1065-1119	ACCATGCGCCGGAACA CCACCCGGAGCTTGTGATT
RPL4 mouse	NM_024212.4	28-97	CTTCTCCTCTCCCCGTCATG GATGACTCTCCCTTTTCGGAGTAC
RC3H1 human	NM_001300850.1	3295-3364	CCACAAAACAAGGTTCCGGC AGGCTGATCCATTTGGTACATCA
RC3H1 mouse	NM_001024952.2	2971-3066	AGGAACGAGAGAGCAGAGGT CGAGAGACTGTTGGTCGGTC
RC3H2 human	NM_001100588.3	3683-3753	AGACCATGTGATTCTGGAGGAG CTGGGAGTGGCTGGCTAAAG
RC3H2 mouse	NM_001100591.1	1750-1828	CTCAGCTAATCCCACGAGGC TTAGTGCCAACCTTCCCGAC
ZC3H12B human	NM_001010888.3	2004-2075	ATTCTAAGCAAGGCCCCAC TTCCAGTTGATGGGTGCTGG
ZC3H12C human	NM_033390.2	1309-1396	ATTACCATCCCGAAAGGGGC GCAGTTTTGGCTGCCGTATT
ZC3H12D human	NM_207360.3	621-702	GCTGTTGACTGGTTCAGGGA CAGCTCTTGGTGGGTCCTTC
<b>Validation of HAP1 cell knockouts</b>			
<i>ZC3H12A</i>	NC_000001.11	37475438-37475770	CTAACCTGTTGGTTGTTTCAGTAGG TGGCTGTCCCGTGTTCAC
<i>ZC3H12B</i>	NM_001010888.3	262-644	TCAGTTGAAGAAAAGGAGATGCAC CTGGCCTCAAATTGTCAGTGTATC
<i>ZC3H12C</i>	NM_033390.2	146-353	CGCCACCTTTATGTGGAGA GCCTGGCTCTACTGAAATGC
<i>RC3H1</i>	NC_000001.11	173983327-173983725	GCAAAGAAGTGGCTTTGTACATCA AGAAGAATTGCTCCTGGACTGTAAA
<i>RC3H2</i>	NC_000009.12	122890211-122890576	ATATAAAGACGGGTTGAGTCTCAGG TTAGCTCCCTTTGTTTCCCTTTTC

## Transparent Methods

A description of the key resources including antibodies, cell lines, oligonucleotides, recombinant DNA, and software are indicated in Table S1.

### Cell lines and culture conditions

HAP1 cells were grown in IMDM (Gibco, 12440-053) plus 10% FBS (Millipore-Sigma, F0926); HUVEC in EBM-2 (Lonza, CC-3156); and the L-M and MEF cells in DMEM (Gibco, 11995-065) plus 10% FBS. Growth surfaces for the HUVEC and MEF cultures were treated with 0.2% gelatin (Millipore-Sigma, G-2500) in PBS for 30 min immediately prior to use. The HAP1 knockout cell lines were validated by sequence analysis of the RT-PCR product generated from total RNA using primers flanking the region of the genomic change (Table S2). The *RC3H1* knockout has a 1 bp insertion (A) in exon 3 (chr1: 173983544); the *RC3H2* knockout has a 1 bp insertion (C) in exon 4 (chr9: 122890422); the *ZC3H12A* knockout has a 16 bp deletion (CCGGAAGCTGGGCTAT) in exon 2 (chr1: 37475649); the *ZC3H12B* knockout has a 47 bp insertion (GGGCCACCTGCATTGGGAGCATGGAGTCAACCACTGGATCGCCAG GT) in exon 1 (chrX: 65489128); and the *ZC3H12C* knockout has a 1 bp insertion (T) in exon 2 (chr11: 110136841). All cultures were maintained at 37 °C in a 5% CO<sub>2</sub> environment within a humidified tissue culture incubator.

### siRNA transfections

HAP1 and HUVEC cells were plated at 120,000 cells per 3.5 cm plate, and the L-M and MEF cells at 80,000 cells per plate. Cells were transfected 24 h later with 10 nM of the appropriate siRNA(s) using Lipofectamine RNAiMAX (Thermo Scientific, 13778) in a final volume of 1.2 ml. Silencer Select negative controls #1 and #2 were used for the assays; both behave similarly. For assays in which siRNAs targeting both *RC3H1* and *RC3H2* were combined, the two negative controls were also combined, and each used at a final concentration of 10 nM. Otherwise, control #2 was used at 10 nM for all assays. After 45 h, the transfection media was replaced with fresh media or with fresh media containing either 100 μM DFO or FAC. The FAC concentration was adjusted for some of the cell types to limit toxicity: HAP1 and L-M cultures contained 100 μg/ml FAC; HUVEC contained 15 μg/ml FAC; and MEFs contained 30 μg/ml FAC. Total RNA was isolated after a 5 h incubation unless otherwise indicated.

### RNA extraction and RT-qPCR assays

Cells were briefly rinsed with PBS (4 °C) prior to directly scraping into 1 ml TRI-reagent to isolate total RNA (Chomczynski and Sacchi, 2006). If the RNA was prepared from cells that had been transfected with a plasmid expressing an amplicon to be quantified, it was further treated with DNase (Promega, M610A). The DNase treatment consisted of 800 ng of the resuspended RNA and 4 units of DNase at 37 °C for 30 min. After extraction of the samples with phenol-chloroform and precipitation of the aqueous phase in ethanol, the pellets were resuspended in dH<sub>2</sub>O. Annealing reactions for the cDNA consisted of 75 ng of the total RNA and 90 ng of a random decamer in a 6 μl volume containing 5 nmol of each standard deoxynucleotide triphosphate (dNTP). The RNA-primer mixtures were heated at 65 °C for 5 min followed by the addition of 2 μl 5x Superscript III buffer (Thermo Scientific 18080-044) and 1 μl 0.1 M DTT while on ice. After a 2 min equilibration at 25 °C, 150 units of Superscript III were added to initiate the reverse transcriptions. The reactions were incubated at 25 °C for 10 min, followed by 42 °C for 50 min. After terminating the reactions by heating at 95 °C for 10 min, the cDNA was diluted with an equal volume of 0.5 μg/μl tRNA (Roche, 10109541001). The qPCR was performed in a 10 μl volume within 96 well plates and each reaction contained 1 μl of the cDNA, 100 nM of the appropriate primers (Table S2), and 5 μl SYBR Green mix (Thermo Scientific, 4309155). Amplification was with a StepONE Plus thermal cycler (Thermo Scientific). The thermal profile consisted of an initial 10 min 95 °C denaturation followed by 40 cycles of a 15 second 95 °C denaturation and a 1 min 65 °C extension. Minus reverse transcriptase controls consistently indicated less than 1% genomic DNA contamination. The  $\Delta\Delta Cq$  method was used to quantify changes in the mRNA amplicons relative to a RPL4 reference unless otherwise indicated. The amplification efficiencies were all close to 95%. All values were calculated from three sets of biological replicates, which were each assayed in triplicate.

## Immunoblot assays

Cells were grown on 3.5 cm plates as already described and treated with either 20  $\mu$ M mepazine or 100  $\mu$ M DFO for 5 h where indicated. Cells were rinsed briefly with PBS (4 °C) prior to directly scraping into 100  $\mu$ l lysis buffer (100 mM Hepes pH 7.5, 2 mM  $MgCl_2$ , 100 mM NaCl, 8 mg/ml protease inhibitors (Thermo Scientific, A32955), 0.4% deoxycholate, 0.8% NP40 and 0.08% sodium dodecyl sulfate). The lysate was left on ice for 10 min prior to clarification at 15,000 x g for 5 min. Protein concentrations were determined using bicinchoninic acid (BCA) assays. Supernatant (10-40  $\mu$ g) was combined with an equal volume of 2X Tris-glycine SDS loading dye containing 10 mM dithiothreitol and heated at 95 °C for 5 min prior to loading on a 10% Tris-glycine gel (Thermo Scientific, XP00100), followed by electroblotting onto Immobilon transfer membrane (Millipore-Sigma, IPFL07810). Electroblotting was for 2 h at 30 volts in Tris-glycine transfer buffer. Methanol was omitted from the transfer buffer for blots involving Roquin to facilitate more efficient transfer. Membranes were dried for 12 h and then treated for 1 h with TBS blocking buffer (Li-Cor) prior to incubating with the primary antibodies (Table S1). The  $\alpha$ -TFR1 and  $\alpha$ -Regnase-1 antibodies were diluted 500-fold in blocking buffer, and all other primary antibodies were diluted 1000-fold. All secondary antibodies were diluted 10,000-fold. Blots were scanned with an Odyssey (Li-Cor) infrared imager and quantified using Image Studio Lite version 5.2.5 (Li-Cor). Scan intensities were adjusted to avoid saturation. Two different sources of protein standards were used in the study: GE Healthcare RPN800E, which includes 38, 52, 76, 102 and 150 kDa proteins; and Thermo Scientific 26616, which includes 40, 55, 70, 100, 130 and 180 kDa proteins. The GE 102 kDa protein has an aberrant mobility on the 10% Tris-glycine gels, migrating ~15 kDa slower than the Thermo Scientific 100 kDa protein standard. The other standards within the two sets are consistent.

## Measurement of the Tfr1 mRNA half-life

The HAP1 cells were plated at 120,000 cells per 3.5 cm plate. After 20 h, the media was removed and replaced with 1 ml fresh media. Cells were either directly treated with EU or treated 40 h after siRNA transfection, as described in the previous section. A 200 mM stock EU solution was made in DMSO and 1  $\mu$ l was added to the cells resulting in a final concentration of 200  $\mu$ M. After a 4 h incubation, the media was removed, and the plates were rinsed with fresh media prior to adding either 100  $\mu$ g/ml FAC or 100  $\mu$ M DFO in fresh media. A chase of unlabeled uridine was not included as it was not found to have any effect, presumably because the endogenous uridine is sufficient to outcompete any label remaining after the washout. At the indicated times, total RNA was isolated as described above and a biotin group added through click chemistry (Bao et al., 2018). Biotin-labeled RNA was enriched on Streptavidin conjugated magnetic beads using the Click-it Nascent RNA Capture Kit (Thermo Scientific, C10365). Beads were then resuspended in 13  $\mu$ l dH<sub>2</sub>O containing 180 ng of a random decamer and 10 nmol of each dNTP. The beads were heated at 65 °C for 5 min, briefly cooled on ice and then 4  $\mu$ l of the Superscript III 5x buffer and 2  $\mu$ l of 0.1 M dithiothreitol were added. Samples were equilibrated at 25 °C for 2 min prior to addition of 200 units of Superscript III. The reverse transcription reactions were incubated for a further 10 min at 25 °C and then transferred to a rotation wheel within a 45 °C hybridization oven for 1 h. The reactions were terminated, and the cDNA eluted from the magnetic beads through heating at 85 °C for 5 min. Regular mixing to keep the beads in suspension was performed during all steps. The released cDNA was separated from the magnetic beads and qPCR performed as described above. Control reactions using RNA isolated from cultures treated with DMSO alone instead of the EU indicated that there was less than 1% contamination arising from non-specific binding of the RNA to the Streptavidin beads. The Tfr1 mRNA  $t_{1/2}$  was calculated for each condition as described below in the Quantitation and Statistical Analysis section.

## Plasmids

All of the following DNA sequences were synthesized at GenScript and confirmed by Sanger sequencing at the University of Minnesota Genomics Center:

### a) *RC3H1* expression plasmids

The complete coding sequence for human *RC3H1* (nt 88-3492 of NM\_001300850) was optimized for expression using Gensmart Codon Optimization software (Genscript) and cloned into the pSF-CMV-NEO-NH2-3xFlag vector (Millipore-Sigma) using EcoRI and KpnI sites. Mutations were likewise introduced into the RNA binding site by chemical synthesis to generate K239A,R260A.

#### b) Stem-loop luciferase-TfR1 reporter plasmid

A strong stem-loop was cloned 4 nt upstream of the start codon of the firefly luciferase gene within the pmirGLO vector. The firefly luciferase gene contains the optimized TfR1 instability sequence within its 3'-UTR (Rupani and Connell, 2016). The strong stem-loop was previously demonstrated to effectively inhibit translation when inserted into other mRNAs (Doma and Parker, 2006): 5'-GAT ATC CCG TGG AGG GGC GCG TGG TGG CGG CTG CAG CCG CCA CCA CGC GCC CCT CCA CGG GAT ATC-3'. The stem loop was synthesized with flanking pmirGLO vector sequence so that it could be cloned into the vector using unique PpuMI and Apal sites. A strong stop during the Sanger sequencing reactions confirmed the presence of the hairpin in the plasmid, and it was also possible to verify 12 nt of the hairpin before the sequencing reactions completely terminated.

#### EMSA

The wildtype and  $\Delta C$  IREs were transcribed from synthetic oligodeoxynucleotide templates using T7 RNA polymerase and then purified on a denaturing 8% polyacrylamide gel (Milligan and Uhlenbeck, 1989). The specific activity of the radiolabeled IRE was approximately  $2 \times 10^4$  dpm/pmol. An RNA solution containing 0.5  $\mu$ M radiolabeled IRE and where indicated 10  $\mu$ M unlabeled competitor was heated at 65 °C for 3 min. One  $\mu$ l of the RNA solution was then added to 9  $\mu$ l of the appropriate cellular extract, which contained approximately 15  $\mu$ g protein. The cellular extracts were prepared from HAP1 wildtype and *RC3H1* KO cells that were grown on 3.5 cm plates, transfected with siRNAs, and treated with FAC or DFO as already described. Cells were rinsed briefly with PBS (4 °C) and directly scraped into 75  $\mu$ l lysis buffer (1 mM DTT, 5% glycerol, 10 mM Hepes pH 7.5, 40 mM KCl, 3 mM MgCl<sub>2</sub>, 0.2% NP40, and 8 mg/ml protease inhibitors). The lysate was left on ice for 10 min prior to clarification at 15,000 x g for 5 min. The RNA binding reactions were incubated for 25 min at room temperature prior to addition of 1  $\mu$ l 500  $\mu$ g/ml heparin. Tubes were left a further 5 min prior to addition of 1  $\mu$ l 95% glycerol containing 0.1% bromophenol blue. Samples were loaded onto a 6% acrylamide/ 0.074% bis-acrylamide gel (0.75 mm thick). Electrophoresis was in 0.5 x TBE (0.045 M Tris-borate, 0.5 mM EDTA) at 10 V/cm for 1 h. The gels were dried onto DE 81 paper (Whatman) and scanned using a Typhoon FLA 9500 (GE Healthcare).

#### Luciferase assays

HAP1 cell lines were plated at 10,000 cells per well within 96-well plates. The siRNA transfections, where indicated, were performed 24 h later as described above for the 3.5 cm plates but scaled to the 96-well plate surface area. Cells were transfected 30 h after the siRNA transfections with either 30 ng of the wildtype or mutated firefly luciferase-TfR1 reporter plasmid using 0.3  $\mu$ l Lipofectamine 2000 in a 75  $\mu$ l final volume. The transfections also included 20 ng of either the wildtype or mutated (K239A, R260A) Roquin expression vector where indicated. Transfection efficiency was estimated by transfection with a  $\beta$ -galactosidase expressing plasmid and subsequent staining with the X-Gal substrate (Thermo Scientific, 45-0450). After 18 h, the luciferase activity was assayed using Dual-Glo reagents (Promega, E2920) and quantified with an Infinite M1000 plate reader (Tecan). Variation in transfection efficiency was controlled by normalization to a *Renilla* luciferase, encoded on the same pmirGLO plasmid as the firefly-TfR1 reporter. Each reporter construct was assayed with three independent sets of transfections, and each set was assayed in at least triplicate.

#### Quantitation and Statistical Analysis

To calculate the  $t_{1/2}$  for the TfR1 mRNA, linear regression models were initially used to determine the slope of the lines for each condition in Figure 2B. The  $R^2$  for the linear regression was reported as an indicator of the goodness of the fit (Table 1). For the FAC treated HAP1 (parental), *ZC3H12A* KO, *ZC3H12B* KO and *ZC3H12C* KO cells, the fit did not include the 7 h time point, as the instability appeared to plateau after 5 h, similar to that previously reported with the L-M cells (Mullner and Kuhn, 1988). The initial time point was not used for the analysis of the DFO treated cells as there appeared to be a transient increase in TfR1 mRNA abundance up to 3 h. The inclusion of the 17.5 h timepoints for the calculation of the slopes with the HAP1-DFO treatment and *RC3H1* knockout/*RC3H2* knockdown did not significantly impact the absolute values, but it did tighten the 95% confidence intervals. The slope from each curve fit corresponds to the negative value of the first order rate constant, and under this condition  $t_{1/2} = \ln(2)/k$ . The 95% confidence interval of the slope was likewise used to derive a confidence interval for the  $t_{1/2}$ . The

analysis was performed using the R programming language. Statistical significance for all other assays was analyzed by a two-tailed Student's t-test. All assays were performed with at least three biological replicates.

### **Supplemental References**

Bao, X., Guo, X., Yin, M., Tariq, M., Lai, Y., Kanwal, S., Zhou, J., Li, N., Lv, Y., Pulido-Quetglas, C., *et al.* (2018). Capturing the interactome of newly transcribed RNA. *Nat Methods* *15*, 213-220.

Chomczynski, P., and Sacchi, N. (2006). The single-step method of RNA isolation by acid guanidinium thiocyanate-phenol-chloroform extraction: twenty-something years on. *Nat* *1*, 581-585.

Milligan, J.F., and Uhlenbeck, O.C. (1989). Synthesis of small RNAs using T7 RNA polymerase. *Methods Enzymol* *180*, 51-62.